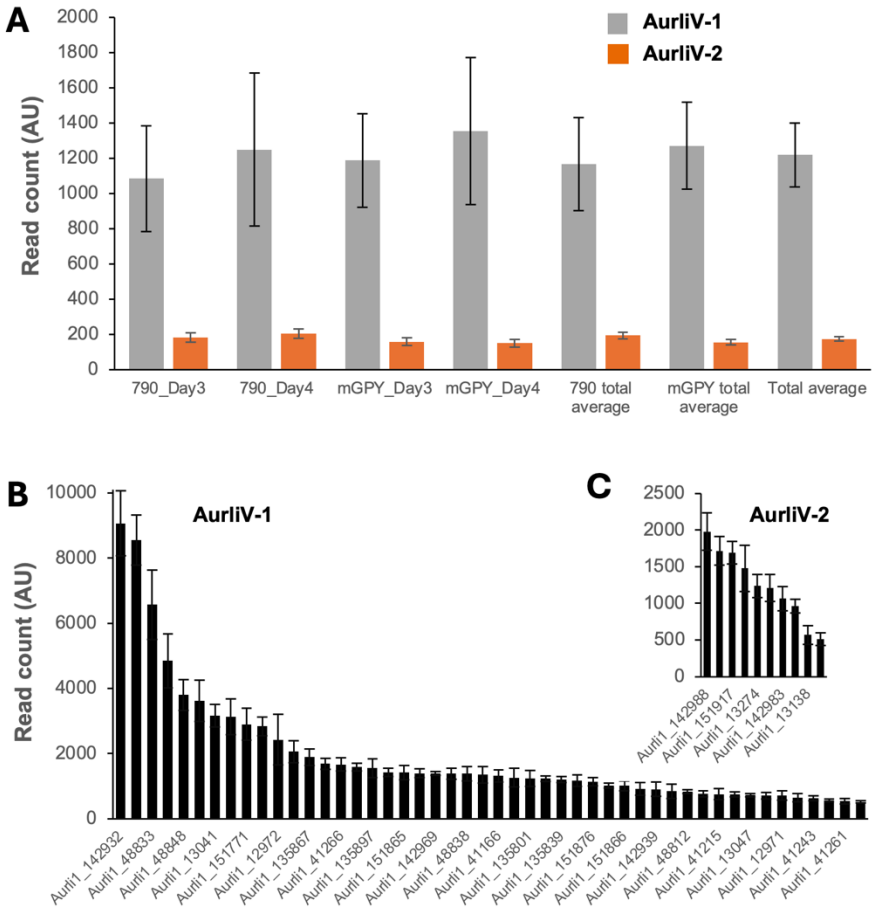

Fig. S1. RNA-seq analysis of mirusvirus gene expression in *Aurantiochytrium limacinum* cultures grown in two rich growth media, 790 BY+ and mGPY. **(A)** Average RNA-seq read counts of all predicted AurliV-1 (episomal) and AurliV-2 (chromosomally integrated) genes. Error bars indicate standard error across three replicates. **(B)** Average RNA-seq read counts of AurliV-1 genes with expression greater than 500 AU; the most highly expressed gene (Aurli1_48845) was omitted due to its exceptionally high expression level (103637.70 AU, standard error of 11151.73 AU). **(C)** Average RNA-seq read counts of genes for AurliV-2 genes with expression greater than 500 AU; error bars indicate standard error over three replicates.

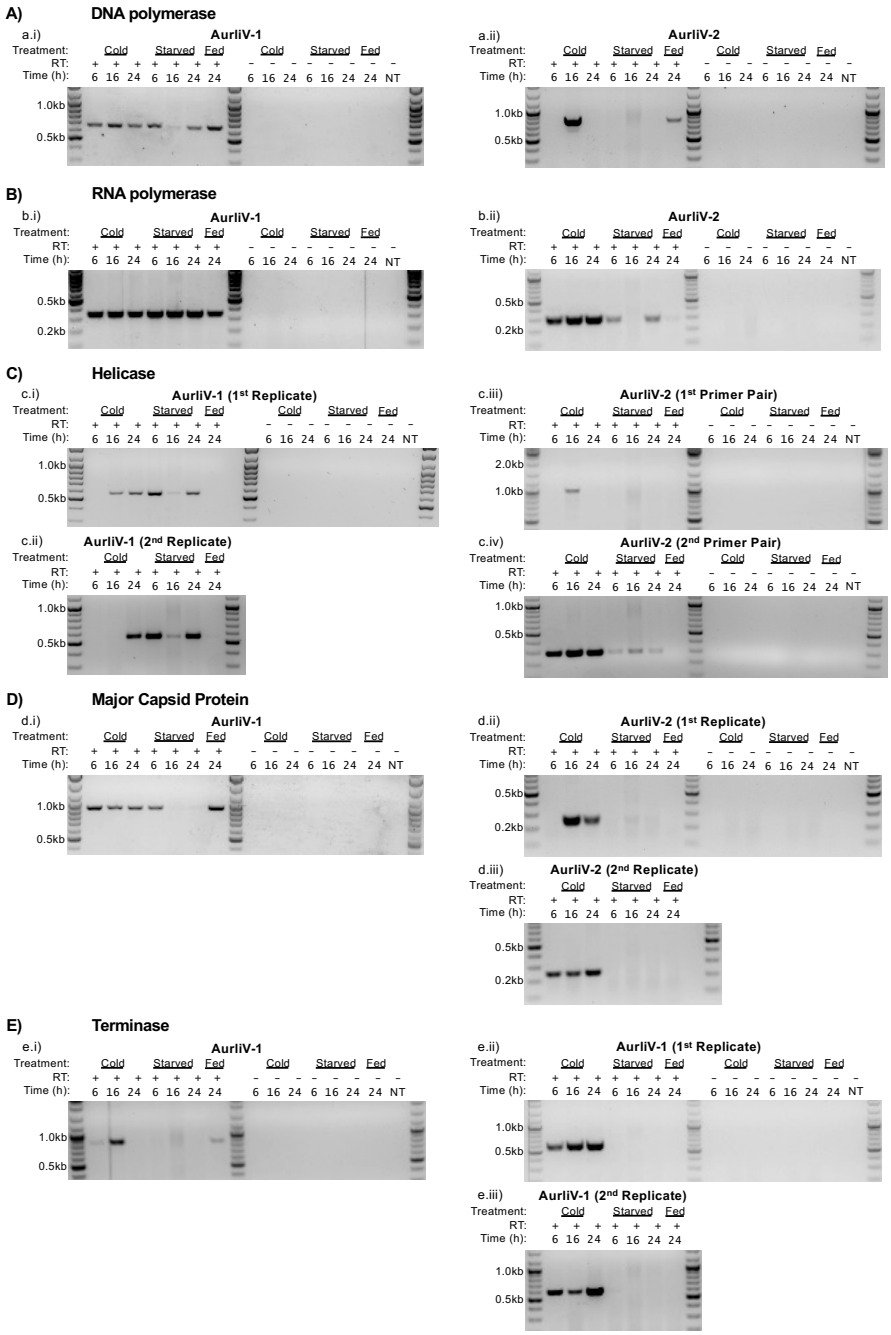

Fig. S2. Gene expression of mirusviral genes in *Aurantiochytrium limacinum* under stress. Data shown are RT-PCR amplifications for five mirusvirus genes at 6-, 16- and 24-hr time points for cold-shocked and starved cultures, with control (fed) cells at 24-hours. **(A)** DNA polymerase expression for AurliV-1 (episomal mirusvirus genomic element; left) and AurliV-2 (chromosomally integrated mirusvirus genomic element;

right). The remaining panels show expression of **(B)** RNA polymerase, **(C)** Helicase, **(D)** Major Capsid Protein, and **(E)** Terminase genes for AurliV-1 (left) and AurliV-2 (right). For the AurliV-2 Helicase gene (C), the right panel shows expression of short (c.iii) and long (c.iv) transcripts to account for two possible start codons. Where shown, multiple RT-PCR replicates were carried out. Controls without reverse transcriptase (No RT '-') and without template (No TP) were performed for all genes and RT-PCR reactions.

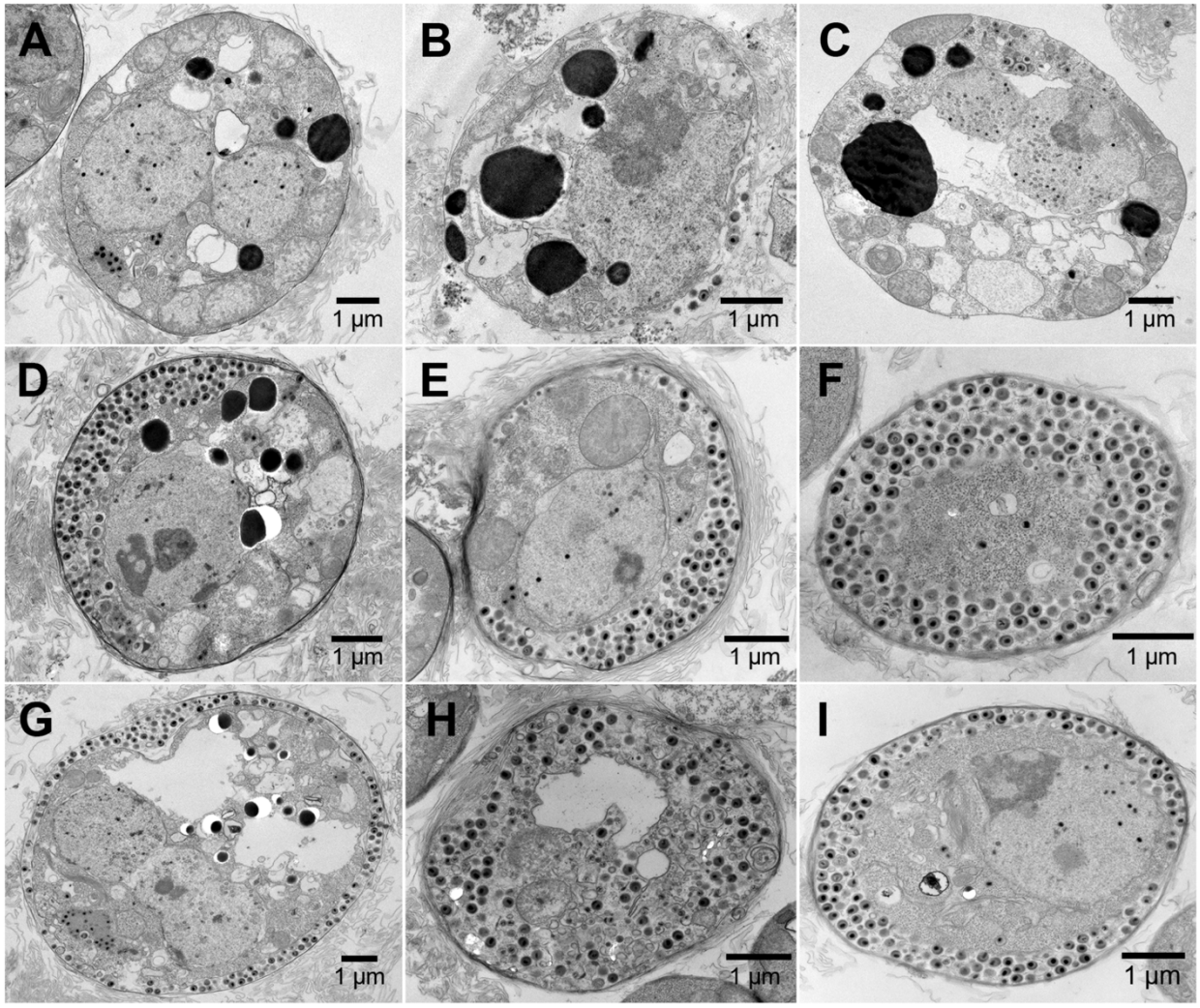

Fig. S3. Representative TEM images of virus-producing *Aurantiochytrium limacinum* cells grown in rich medium (790 By+) for 26 h (**A-C**) and under starvation conditions (**D** and **E**, artificial sea water (ASW) for 19 h, **F-I**, ASW for 26 h). Accumulation of virus particles between the plasma membrane and cell wall is prominent in starved cells (F-I) and can occasionally be seen in control cells (B). Large electron-dense regions present in A-D correspond to lipid droplets.

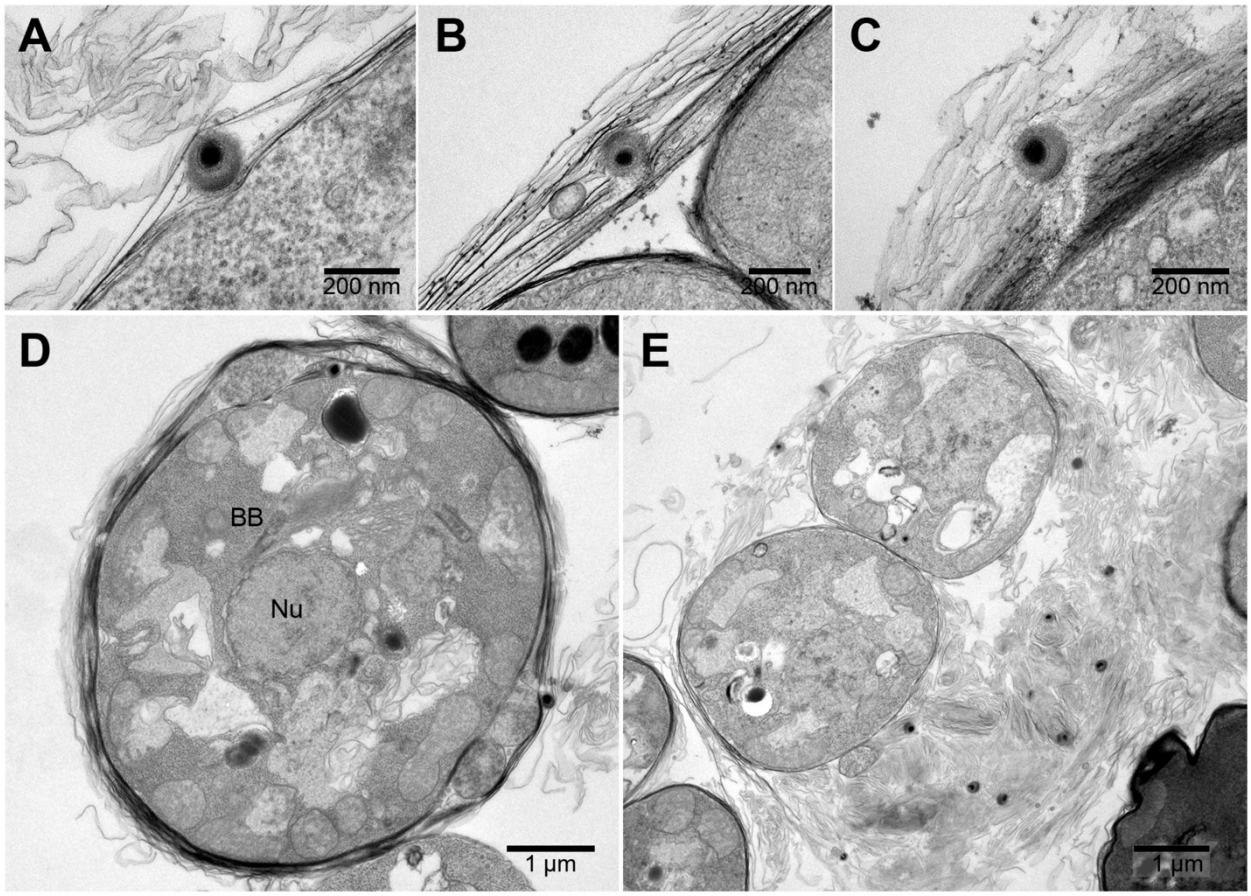

Fig. S4. Representative images of virus-like particles in *Aurantiochytrium limacinum* from starvation conditions (artificial seawater cultures). **(A-C)** Mirusvirus particles between cell wall layers. **(D)** Mirusvirus particle at the cell wall of a putative zoospore. BB = basal body, Nu = nucleus. **(E)** Mirusvirus particles attached to layers of a disintegrating cell wall.

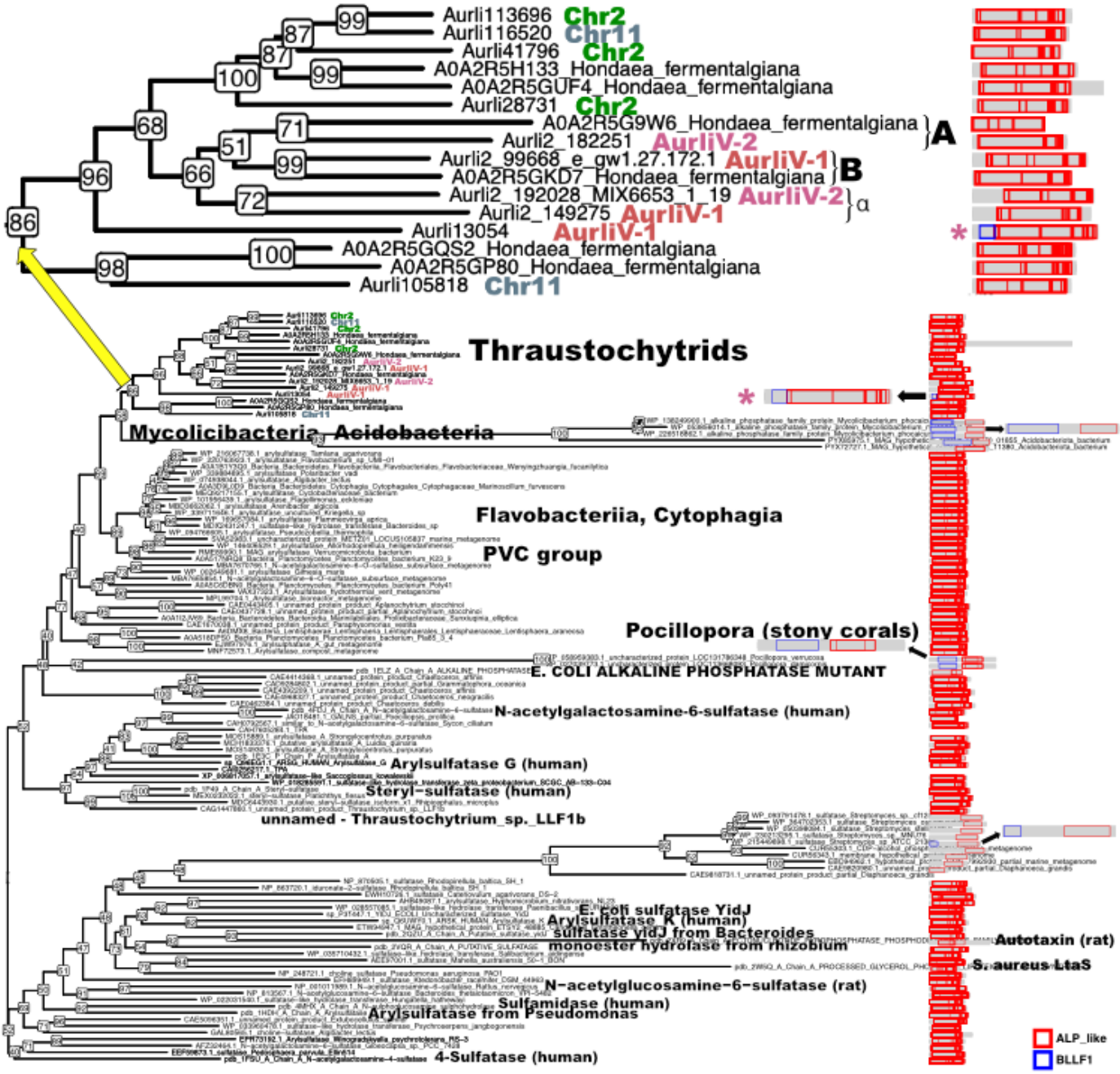

Fig. S5. Maximum likelihood phylogeny of proteins with arylsulfatase-like (ALP-like) domains. Colored boxes at right indicate the organization of BLLF1 and ALP-like and domains within each protein; representative proteins with both domains are expanded. Ultrafast bootstrap support values are shown at nodes. **Top**: zoomed-in view of thraustochytrid ALP-like domain genes, including the chromosomal location of each gene; the fusion protein of interest is marked with an asterisk.

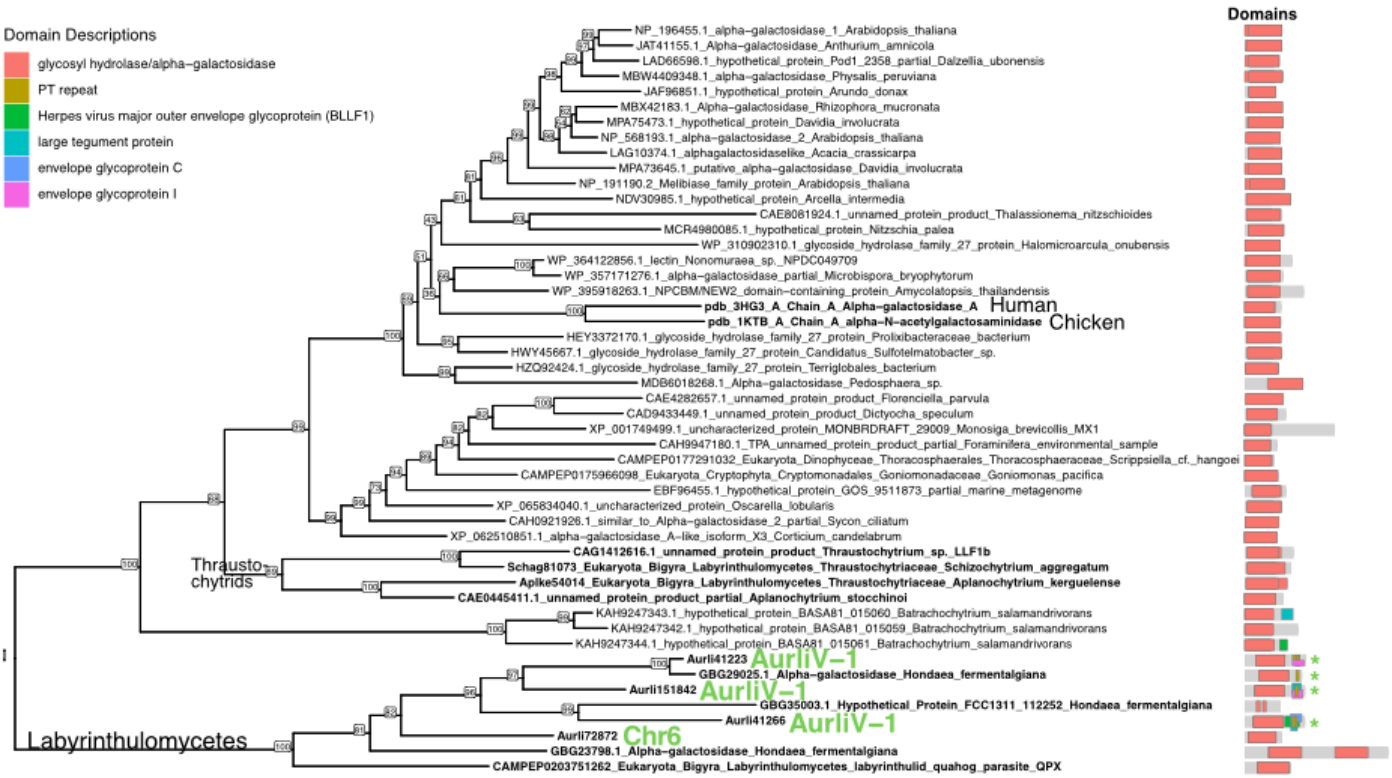

Fig. S6. Maximum likelihood phylogeny of proteins with alpha-galactosidase domains. Colored boxes at right indicate the organization of arylsulfatase and viral glycoprotein-like domains within each protein. Ultrafast bootstrap support values are shown at nodes. Proteins encoded on the AurliV-1 chromosome and chromosome 6 of *A. limacinum* are labelled; fusion proteins of interest are marked with an asterisk.